ELSEVIER

Journal of Biomechanics 38 (2005) 657–665

JOURNAL OF BIOMECHANICS

www.elsevier.com/locate/jbiomech
www.JBiomech.com

Journal of Biomechanics Award

A 3D model of muscle reveals the causes of nonuniform strains in the biceps brachii

Silvia S. Blemker[a], Peter M. Pinsky[a], Scott L. Delp[a,b,*]

[a] *Department of Mechanical Engineering, Stanford University, Stanford, CA, USA*
[b] *Department of Bioengineering, Stanford University, Stanford, CA, USA*

Accepted 4 April 2004

Abstract

Biomechanical models generally assume that muscle fascicles shorten uniformly. However, dynamic magnetic resonance (MR) images of the biceps brachii have recently shown nonuniform shortening along some muscle fascicles during low-load elbow flexion (J. Appl. Physiol. 92 (2002) 2381). The purpose of this study was to uncover the features of the biceps brachii architecture and material properties that could lead to nonuniform shortening. We created a three-dimensional finite-element model of the biceps brachii and compared the tissue strains predicted by the model with experimentally measured tissue strains. The finite-element model predicted strains that were within one standard deviation of the experimentally measured strains. Analysis of the model revealed that the variation in fascicle lengths within the muscle and the curvature of the fascicles were the primary factors contributing to nonuniform strains. Continuum representations of muscle, combined with in vivo image data, are needed to deepen our understanding of how complex geometric arrangements of muscle fibers affect muscle contraction mechanics.

Keywords: Skeletal muscle; Finite-element modeling; Muscle architecture; Upper limb; Fascicle geometry

1. Introduction

Skeletal muscle has a complex hierarchical organization in which thousands of force-producing muscle fibers are arranged within a connective tissue network. The properties of individual fibers have been studied in isolation over the last four decades (e.g., Gordon et al., 1966; Denoth et al., 2002). However, how the behaviors of muscle fibers may change once they are arranged within muscle is not well understood. Therefore, "lumped-parameter" models, which assume that all fibers act independently and shorten uniformly, are used to mathematically represent whole muscle.

Recent experimental studies have reported nonuniform shortening along fascicles (bundles of fibers) within muscle (Ahn et al., 2003; Pappas et al., 2002; Drost et al., 2003). In one study, dynamic magnetic resonance (MR) images taken of the long head of the biceps brachii showed nonuniform shortening along some muscle fascicles during low-load elbow flexion (Pappas et al., 2002). These data challenge the simplifying assumptions made in lumped-parameter models of muscle and motivate us to identify the features of the biceps architecture that could contribute to nonuniform strains.

Even though the biceps brachii is typically considered to have a parallel-fibered architecture, the fascicles have a more complex geometrical arrangement (Fig. 1) that could potentially contribute to nonuniform shortening. For example, muscle shortening could be affected by the difference in the lengths of the centerline fascicles and the anterior fascicles and/or the curvature of the anterior fascicles (Asakawa et al., 2002). Stretch in passive structures, such as the internal aponeuroses or the external fascia, also has the potential to create complex strain distributions. There is evidence that lateral transmission of tension between fibers is present

*Corresponding author. James H. Clark Center, Room S-321, Stanford University, MailCode: 5450, 318 Campus Drive, Stanford, CA 94305-5450, USA.,Tel.: +650-723-1230; fax: +650-725-1587.
E-mail address: delp@stanford.edu (S.L. Delp).

0021-9290/$ - see front matter © 2004 Elsevier Ltd. All rights reserved.
doi:10.1016/j.jbiomech.2004.04.009

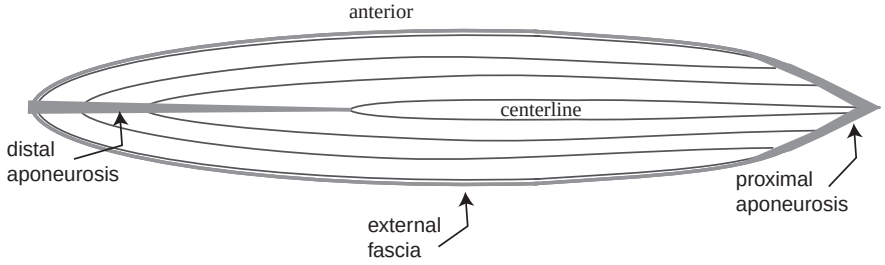

Fig. 1. Simplified schematic of the biceps brachii architecture. The primary passive structures are the proximal aponeurosis, distal aponeurosis, and external fascia. The muscle fascicles potentially are at different lengths and have a slight curvature as they insert into the aponereuroses. Stretch in the aponeuroses, fascicle curvature, variation in fascicle lengths, and external fascia constraints could all potentially contribute to nonuniform strains within the muscle.

(Street, 1983; Trotter, 1993), which plays a significant role in force production and transmission (Huijing, 1999; Purslow, 2002). The resistance to shearing between fibers and muscle volume preservation also affect the tissue deformations. To explore the effects of fascicle geometry and passive structures on the strain distributions, a model that incorporates the fiber properties, volume preservation, shear properties, and detailed fascicle geometry of the biceps muscle is needed.

The purpose of this work was to uncover the features of the biceps architecture that contribute to the nonuniform strains. We developed a new constitutive model for muscle that represents the active and passive muscle fiber characteristics, intramuscular connective tissue properties, and muscle volume preservation. In this model, we used a new set of parameters to characterize tissue deformations that represents transverse properties of the tissue in a novel and intuitive manner. We created a finite-element model that replicated the major features of the biceps brachii muscle internal geometry, simulated the conditions imposed in a previous dynamic imaging study (Pappas et al., 2002), and compared tissue strains in the model with these in vivo data. We then varied the model's fascicle geometry to explore the effects of the architecture on the strain distributions in the muscle. Specifically, we examined the effects of the nonuniform fiber lengths, fascicle curvature, aponeurosis stretch, and external fascia on the distribution of fascicle strains.

2. Methods

2.1. Constitutive model

We modeled muscle as a fiber-reinforced composite with transversely isotropic material symmetry, similar to the approach previously used to represent ligament (Weiss et al., 1996). The model uses an uncoupled form of the strain energy (Simo and Taylor, 1991; Weiss et al., 1996) to simulate the nearly incompressible behavior of muscle tissue. This uncoupled form additively separates the dilatational (Ψ_{vol}) and deviatoric (Ψ_{iso}) responses of the tissue

$$\Psi(\mathbf{C}, \mathbf{a}_0) = \Psi_{\text{iso}}(\bar{I}_1, \bar{I}_2, \bar{I}_4, \bar{I}_5) + \Psi_{\text{vol}}(J) \tag{1}$$

where $\mathbf{C}$ is the right Cauchy–Green deformation tensor, $\mathbf{a}_0$ is the local fiber direction, $\bar{I}_1$ and $\bar{I}_2$ are deviatoric invariants of $\mathbf{C}$, $\bar{I}_4$ and $\bar{I}_5$ are additional deviatoric invariants of $\mathbf{C}$ that arise from the description of transverse isotropy, and J is equal to $\sqrt{\det(\mathbf{C})}$ and is the relative change in volume. The isotropic invariants ($\bar{I}_1$ and $\bar{I}_2$) have been used to represent the underlying "matrix" material. $\bar{I}_4$ equals the square of the local fiber stretch and therefore is commonly used to represent the strain energy within the embedded fibers. However, the other invariants ($\bar{I}_1$,$\bar{I}_2$, and $\bar{I}_5$) do not have a geometrical counterparts, and they couple the material's responses in all directions.

Our goal was to define a strain energy function that separates the material's responses to stretch in the fibers, shearing along fibers, and shearing transverse to the fibers. Representation of stretch in fibers is straightforward, as the standard invariant $\bar{I}_4$ equals the square of the local fiber stretch. To represent the intramuscular connective tissue's resistance to along-fiber and cross-fiber shear, we used two new strain invariants (B_1 and B_2). These invariants (Criscione et al., 2001) represent the along-fiber and cross-fiber shear, respectively (Fig. 2). Therefore, the deviatoric portion of the strain energy (Ψ_{iso}) was described by:

$$\Psi_{\text{iso}}(\bar{I}_1, \bar{I}_4, \bar{I}_5, \alpha) = W_1(B_1(\bar{I}_4, \bar{I}_5)) + W_2(B_2(\bar{I}_1, \bar{I}_4, \bar{I}_5)) + W_3(\lambda(\bar{I}_4), \alpha) \tag{2}$$

where α is the activation level in the muscle, and B_1, B_2, and λ can be expressed in terms of $\bar{I}_1$,$\bar{I}_4$, and $\bar{I}_5$ (Criscione et al., 2001):

$$B_1 = \sqrt{\frac{\bar{I}_5}{\bar{I}_4^2} - 1}, \quad B_2 = \cosh^{-1}\left(\frac{\bar{I}_1\bar{I}_4 - \bar{I}_5}{2\sqrt{\bar{I}_4}}\right), \text{and} \quad \lambda = \sqrt{\bar{I}_4}. \tag{3}$$

These invariants allow for explicit and independent representation of the material's resistance to along-fiber shear and cross-fiber shear.

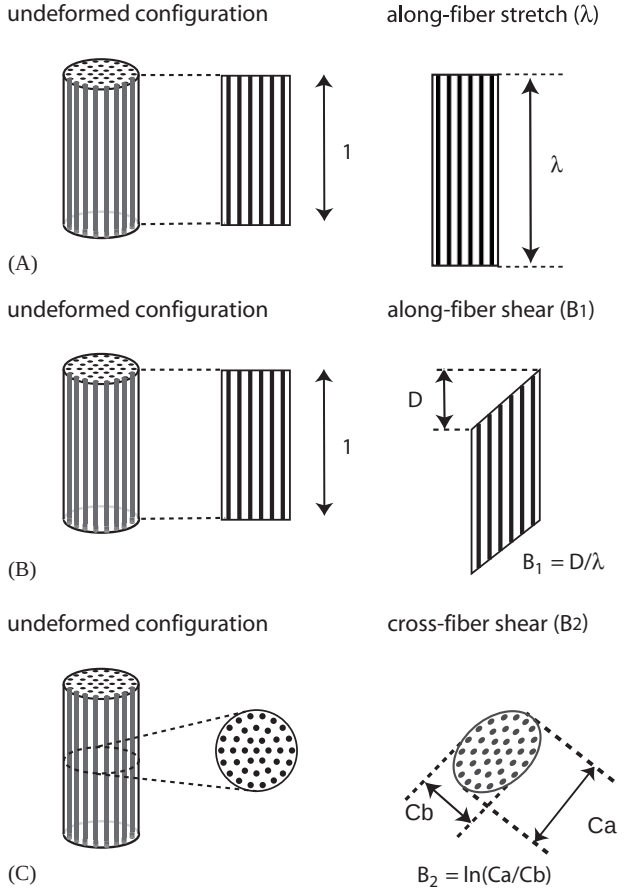

Fig. 2. Strain invariants used to formulate the constitutive model for muscle. The invariants, proposed by Criscione et al. (2001), characterize the along-fiber stretch (A), along-fiber simple shear strain (B), and cross-fiber pure shear strain (C).

The functions W_1 and W_2 represent the along-fiber and cross-fiber strain energies, respectively. The functional forms adopted for our model are as follows:

$$W_1 = G_1(\mathrm{B}_1)^2 \text{ and } W_2 = G_2(\mathrm{B}_2)^2, \tag{4}$$

where G_1 and G_2 represent the effective along-fiber shear modulus and cross-fiber shear modulus, respectively. Eq. (4) were used to represent both muscle and tendon, with different values for constants G_1 and G_2 for each tissue (Table 2).

The term W_3 defines the relationship between Cauchy stress in the fibers ($\sigma^{\text{fiber}}_{\text{total}}$), the fiber stretch ($\lambda$), and the activation level (α):

$$\lambda\frac{\partial W_3^{\text{muscle}}}{\partial\lambda} = \sigma^{\text{fiber}}_{\text{total}}(\lambda,\alpha). \tag{5}$$

To define $\sigma^{\text{fiber}}_{\text{total}}$, we made several assumptions. First, we assumed a normalized force-length relationship ($f^{\text{fiber}}_{\text{total}}$) of a muscle fiber (Zajac, 1989). Second, we assumed a maximum isometric stress ($\sigma_{\max}$) occurs at the optimal fiber stretch (λ_{ofl}), which defines the fiber stretch at which sarcomeres reach optimal length. Lastly, we assumed that the active fiber stress scales linearly with the activation level (α), which varies from 0 (no activation) to 1 (maximal activation):

$$\sigma^{\text{fiber}}_{\text{total}}(\lambda,\alpha) = \sigma_{\max} f^{\text{fiber}}_{\text{total}}(\lambda,\alpha)\lambda/\lambda_{\text{ofl}}. \tag{6}$$

Eq. (6) reflects the fact that, throughout a deformation, the maximum possible stress changes as a result of a change in cross-sectional area of the fibers (see the appendix for a derivation of this relationship).

The normalized function for total fiber force ($f^{\text{fiber}}_{\text{total}}$), which is a function of the fiber stretch, was assumed to be the sum of the passive fiber force ($f^{\text{fiber}}_{\text{Passive}}$) and active fiber force ($f^{\text{fiber}}_{\text{active}}$):

$$f^{\text{fiber}}_{\text{total}}(\lambda,\alpha) = f^{\text{fiber}}_{\text{passive}}(\lambda) + \alpha f^{\text{fiber}}_{\text{active}}(\lambda). \tag{7}$$

A piecewise exponential form was assumed for the passive fiber force, and a piecewise quadratic form was assumed for the active fiber force (see Table 1 for expressions for $f^{\text{fiber}}_{\text{passive}}$ and $f^{\text{fiber}}_{\text{active}}$).

We also defined W_3 for tendinous tissue (aponeurosis and external fascia) using a function that characterized the relationship between the Cauchy stress in the tendon (σ^{tendon}) and the fiber stretch (λ):

$$\lambda\frac{\partial W_3^{\text{tendon}}}{\partial\lambda} = \sigma^{\text{tendon}}(\lambda). \tag{8}$$

The expression for (σ^{tendon}) (Table 1) and the associated material constants (Table 2) were defined to be consistent with the published stress–strain relationship for tendon (Zajac, 1989).

Table 1
Constitutive Model Equations

Normalized passive fiber force $f^{\text{fiber}}_{\text{passive}}(\lambda)$[a], *see* Eq. (7)	
$f^{\text{fiber}}_{\text{passive}}(\lambda) = 0$	$\lambda \leqslant \lambda_{\text{ofl}}$
$f^{\text{fiber}}_{\text{passive}}(\lambda) = P_1(e^{P_2(\lambda/\lambda_{\text{ofl}}-1)} - 1)$	$\lambda_{\text{ofl}} < \lambda < \lambda^*$
$f^{\text{fiber}}_{\text{passive}}(\lambda) = P_3\lambda/\lambda_{\text{ofl}} + P_4$	$\lambda \geqslant \lambda^*$
Normalized active fiber force $f^{\text{fiber}}_{\text{active}}(\lambda)$, *see* Eq. (7)	
$f^{\text{fiber}}_{\text{active}}(\lambda) = 9(\lambda/\lambda_{\text{ofl}} - 0.4)^2$	$\lambda \leqslant 0.6\lambda_{\text{ofl}}$
$f^{\text{fiber}}_{\text{active}}(\lambda) = 9(\lambda/\lambda_{\text{ofl}} - 1.6)^2$	$\lambda \geqslant 1.4\lambda_{\text{ofl}}$
$f^{\text{fiber}}_{\text{active}}(\lambda) = 1 - 4(1 - \lambda/\lambda_{\text{ofl}})^2$	$0.6\lambda_{\text{ofl}} < \lambda < 1.4\lambda_{\text{ofl}}$
Aponeurosis and external fascia along-fiber Cauchy stress $\sigma^{\text{tendon}}(\lambda)$[b], *see* Eq. (8)	
$\sigma^{\text{tendon}}(\lambda) = 0$	$\lambda \leqslant 1.0$
$\sigma^{\text{tendon}}(\lambda) = L_1(e^{L_2(\lambda-1)} - 1)$	$1.0 < \lambda < \lambda^*$
$\sigma^{\text{tendon}}(\lambda) = L_3\lambda + L_4$	$\lambda \geqslant \lambda^*$

[a] λ^* here represents the fiber stretch at which the $f^{\text{fiber}}_{\text{passive}}$ becomes linear. P_3 and P_4 are defined so that $f^{\text{fiber}}_{\text{passive}}$ is C0 and C1 continuous at $\lambda = \lambda^*$.

[b] λ^* here represents the fiber stretch at which σ^{tendon} becomes linear. L_3 and L_4 are defined so that σ^{tendon} is C0 and C1 continuous at $\lambda = \lambda^*$.

The definition of Ψ_{vol} was the same as that used by Weiss et al. (1996), representing the nearly incompressible behavior of biological tissues:

$$\Psi_{vol} = \frac{K}{2}\ln(J)^2, \quad (9)$$

where K is the effective bulk modulus of the tissue. It has been shown that prescription of K to be 1000 times the shear modulus of the tissue will result in a nearly incompressible behavior, and the strain distributions are not highly sensitive to prescription of the bulk modulus (Gardiner and Weiss, 2001). The constitutive model was implemented in the nonlinear finite-element solver, NIKED (Puso et al., 2002).

2.2. Mesh and fiber map definition

The finite-element hexahedral mesh geometry represented the long head of the biceps muscle tissue, proximal aponeurosis, and the distal aponeurosis (Fig. 3A). The model was axially symmetric about the centerline and included approximately 20,000 linear hexahedral elements.

Table 2
Constitutive Model Parameters

Muscle along-fiber constants		Aponeurosis and external fascia along-fiber constants	
P_1 (dimensionless)	0.05	L_1 (Pa)	2.7E6
P_2 (dimensionless)	6.6	L_2 (dimensionless)	46.4
λ^* (dimensionless)	1.4	λ^* (dimensionless)	1.03
σ_{max}(Pa)	3.0E5		
λ_{ofl} (dimensionless)	1.4		
Muscle transverse constants		**Aponeurosis and external fasciatransverse constants**	
G_1 (Pa)	5.0E2	G_1 (Pa)	5.0E4
G_2 (Pa)	5.0E2	G_2 (Pa)	5.0E4
K (Pa)	1.0E7	K (Pa)	1.0E8

For each element in the mesh, a fiber direction vector was needed for input to the constitutive model (to define $\mathbf{a}_0$ in Eq. (1)). We created a fiber map, based on fascicle arrangement measurements from ultrasound images (Asakawa et al., 2002), that consisted of a set of interpolated cubic splines (Fig. 3B). For each element in the mesh (e^i), we determined the corresponding spline (or "fiber"). The fiber direction ($\mathbf{a}_0^i$) was calculated as the vector tangent to the spline curve at the element's center point.

2.3. Comparison with in vivo data

We compared the average strains estimated with the finite-element model to previously acquired dynamic MR data (Pappas et al., 2002). In that study, cine phase-contrast images were acquired as 12 subjects flexed their elbows while resisting a low load (15% maximum voluntary contraction). Displacements of 1 cm^2 regions (placed along the anterior and centerline regions of the biceps images) were tracked to estimate the change in length (or "strains") between regions as a function of length along the muscle.

To compare the finite-element biceps model with the image data, we generated simulations of the model at 15% activation during a quasi-static 4 cm lengthening. The boundary conditions (Fig. 3) consisted of applying a 4 cm displacement (along z) to the distal end, fixing the proximal end (along z), and imposing symmetry boundary conditions to the interior regions. To visualize the results, we created contour plots of the along-fiber stretch, along-fiber shear strain, and cross-fiber shear strain in the longest state. To compare with the imaging results, we calculated the change in length between nodes along the anterior and centerline regions as a function of the distance along the muscle. In this calculation, the change in length was determined with the long state as the reference. We also calculated the average displacement across 1 cm^2 regions in the model

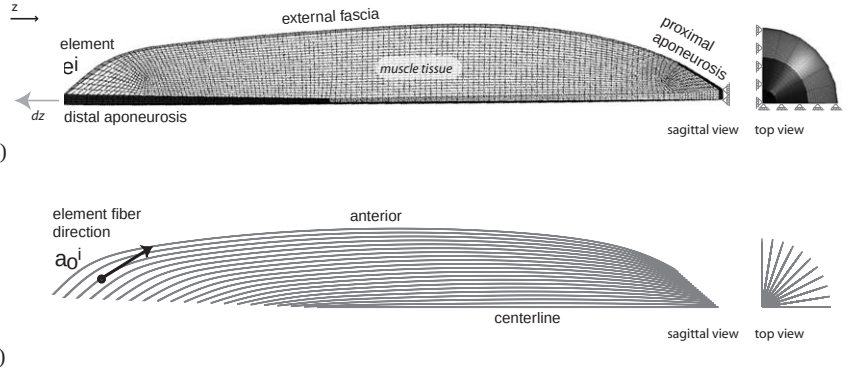

Fig. 3. Mesh (A) and fiber map (B) geometry for the "Original Model," which represents the long head of the biceps brachii. The model is 15 cm long and axially symmetric about the centerline. We applied a 4 cm displacement (dz) to the distal end, fixed the proximal end (along z), and imposed symmetry boundary conditions to the interior regions.

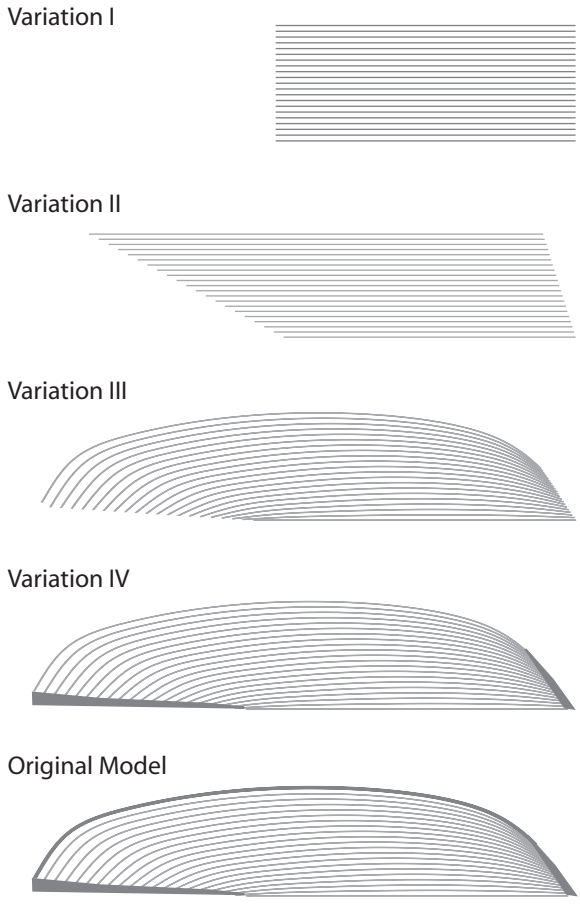

Fig. 4. Schematics of each variation in the model geometry. Variation I has parallel fascicles with equal lengths; Variation II has parallel fascicles with a variation in lengths; Variation III has curved fascicles with a variation in lengths; Variation IV has curved fascicles, variation in lengths, and compliant aponeuroses; and the Original Model adds external fascia to Variation IV.

and determined the change in length along these averaged regions.

2.4. Model variations

To examine the effect of muscle architecture on the strain distributions, we created four models that were each variants (Fig. 4) of the "Original Model" described above (Fig. 3). "Variation I" had uniform parallel fascicles. "Variation II" had a variation in fascicle lengths, but no curvature. "Variation III" had the same fascicle geometry as the Original Model, but had a rigid tendon and no external fascia. "Variation IV" had the same fascicle and tendon geometry as the Original Model, but did not include the external fascia. The boundary conditions applied to Variations I–IV were similar to those applied to the Original Model.

3. Results

The Original Model (Fig. 4) predicted fiber stretch and shear strains that were nonuniform throughout the muscle (Fig. 5). The along-fiber stretch (Fig. 5A) varied from 1.0 (within the tendon) to 1.6 (in the proximal part of the centerline region and distal portion of the anterior region.) The along-fiber shear strains (Fig. 5B) varied from 0.0 to 2.4 and were the highest around the aponeurosis. The cross-fiber shear strains (Fig. 5C) varied from 0.0 to 0.5 and were the highest where the fascicles insert into the aponeurosis.

The changes in length averaged over 1 cm^2 regions in the Original Model were within one standard deviation of the average changes in length measured in 12 subjects (Pappas et al., 2002) for both the anterior and the centerline regions (Fig. 6). Along the centerline region (Fig. 6A), the changes in length varied from 1% to 5% in the aponeurosis elements and from 5% to 35% in the muscle elements. Along the anterior region (Fig. 6B), the change in element length varied from 15% to 25%.

The model with uniform fascicle lengths (Variation I) predicted uniform changes in length along both the anterior and centerline regions (Fig. 7). The model with the different fascicle lengths (Variation II) predicted nonuniform strains along both regions. The model with fascicle curvature (Variation III) had strain distributions that were slightly more nonuniform than those in Variation II. The model with compliant aponeuroses (Variation IV) predicted strains (Fig. 8) that did not differ significantly from the model without aponeurosis compliance. Comparison of Variation IV with the Original Model shows that the external fascia caused the strains along the anterior region to be more uniform, and had little effect on the centerline strains.

4. Discussion

The results of previous in vivo measurements in the biceps brachii showed that the muscle shortens uniformly along the anterior fascicles of the muscle and nonuniformly along the centerline fascicles (Pappas et al., 2002). The purpose of this study was to uncover the features of the biceps brachii muscle architecture that contribute to nonuniform strains along fascicles. Our continuum model of the biceps reproduced the strain distributions observed in vivo. Furthermore, we found that the variation in fascicle lengths and fascicle curvature caused nonuniform fascicle strains in our model.

In addition to nonuniform strains along fascicles, we also observed significant shear strains in the model. It has been suggested (Huijing, 1999; Purslow, 2002) that high along-fiber shear strains (>2.0) occur in complex muscles that undergo large changes in pennation angle

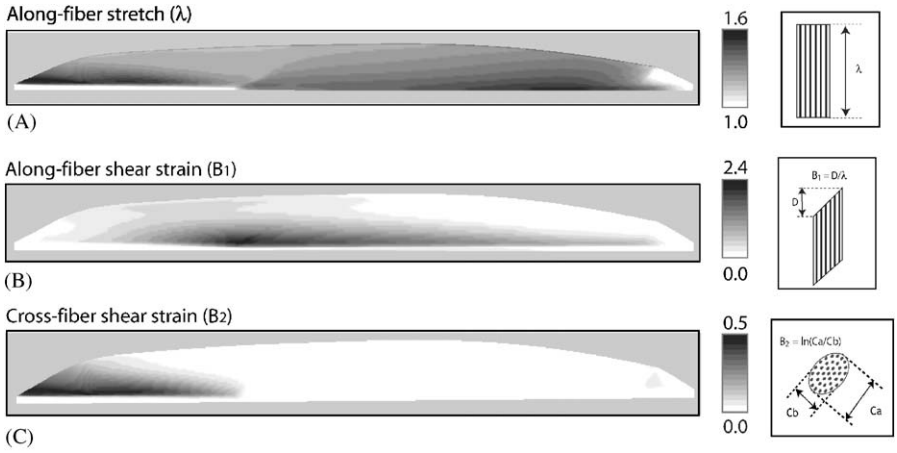

Fig. 5. Contour plots of along-fiber stretch (A), along-fiber shear (B), and cross-fiber shear (C). The along-fiber stretch was highest along the proximal part of the centerline and distal part of the anterior region. The along-fiber shear was highest around the distal aponeurosis. The cross-fiber shears were high only in the distal part of the anterior region.

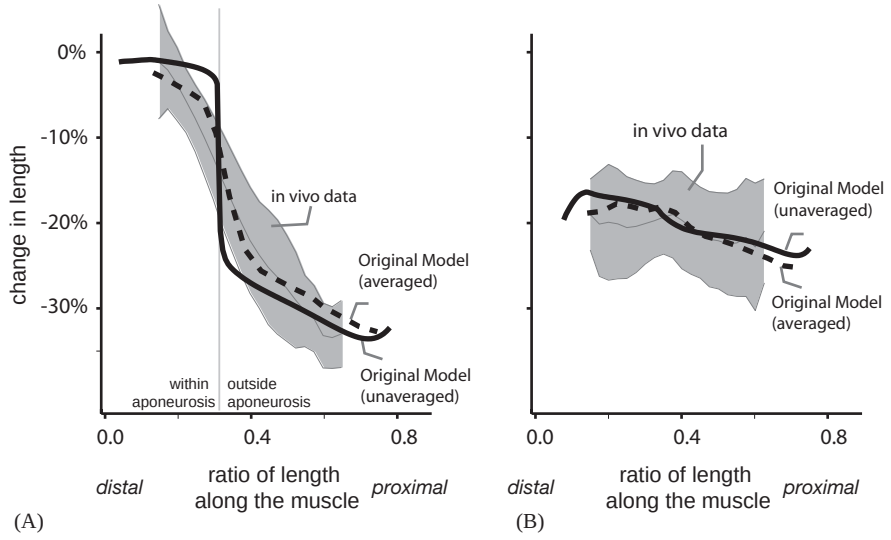

Fig. 6. Change in length between nodes in the Original Model (solid lines), change in length between 1 cm^2 averaged regions in the Original Model (dashed lines), and the image data (shaded regions, average $\pm$ 1 S.D. from Pappas et al., 2002) along the centerline (A) and the anterior (B) regions of the biceps. Percent change in length is plotted as a function of distance from distal tendon, normalized by the length of the biceps brachii long head muscle belly. Negative values of percent change in length indicate muscle shortening with elbow flexion. The degree of nonuniformity in the strains is indicated by the amount of variation in percent change in length along the muscle (i.e., if the strains along each region were uniform, the curves would be horizontal.)

($>40^\circ$). However, in our model we show that high shear strains can occur in muscles without large changes in pennation (5° in our model). Characterization of the shearing behavior between fibers is important because it influences the potential for fibers to transmit force laterally via intramuscular connective tissue (Huijing, 1999; Purslow, 2002). The potential for the intramuscular connective tissue to transmit force laterally has also been demonstrated via measurements of nonlinear force summation across motor units within muscle (Sandercock, 2003) and the observation that some muscle fibers terminate intrafascicularly (e.g., Trotter, 1990).

This paper introduces a novel constitutive formulation for skeletal muscle that is based on strain invariants (Criscione et al., 2001) that allow for direct physical interpretation of deformations. Previous continuum models of skeletal muscle have used two other formulations. The first formulation represents muscle using the standard deformation-coupling invariants ($I_1 - I_5$) for transverse-isotropy (Gielen et al., 2000; Johansson et al., 2000; Martins et al., 1998; Oomens et al., 2003). While some of the invariants (I_3 and I_4) represent geometric quantities (fiber stretch and volume strain, respectively), the other terms (I_1, I_2, and I_5) do not have a geometrical meaning, and they couple the material's response in all

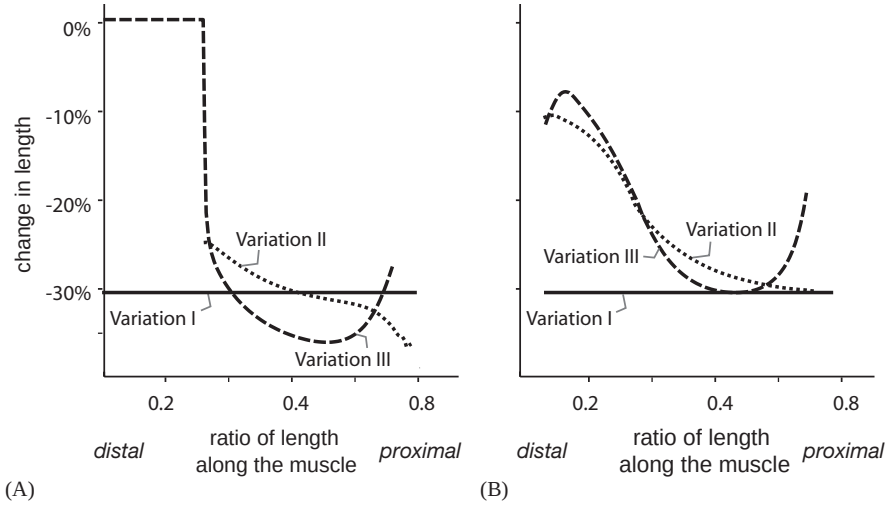

Fig. 7. Strain distributions along the centerline (A) and anterior (B) fascicles in Variations I–III. As expected in the uniform parallel model (Variation I), the strains were uniform along both regions. The nonuniform parallel model (Variation II) predicted nonuniform strains along both the centerline and anterior fascicles (there was nonuniform shortening between the two fascicles and nonuniform along both fascicles). The model with fascicle curvature (Variation III) predicted slightly more nonuniform strains.

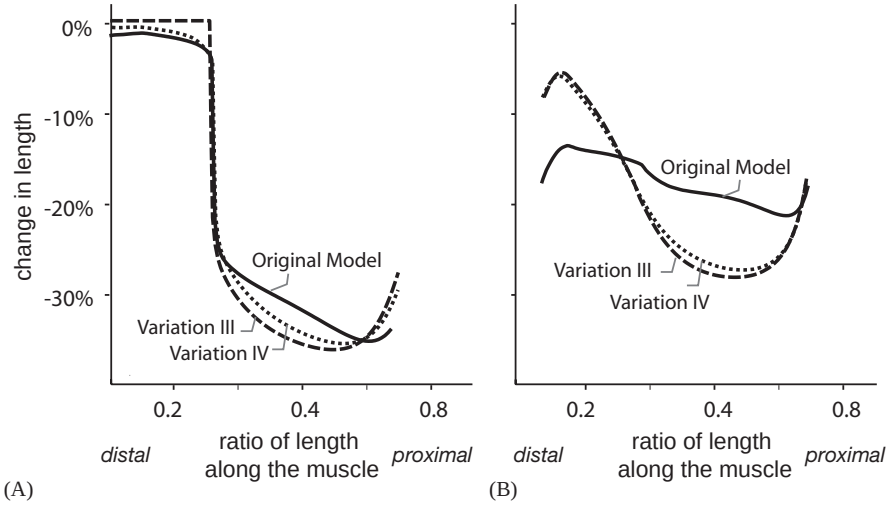

Fig. 8. Strain distributions along the centerline (A) and anterior (B) fascicles in Variations III and IV and the Original Model. The compliant aponeuroses have little effect on the distributions; if anything the aponeuroses create more uniform strains (comparison of Variations III and IV). The external fascia in the Original Model has a slight effect on the centerline strains and large effect on the anterior strains, creating more uniform strains (comparison of Variation IV and the Original Model).

directions. Therefore, it is virtually impossible to define strain energies that explicitly and independently represent intramuscular connective tissue's response to along-fiber and cross-fiber shear. Another approach is to represent muscle as an orthotropic material (Jenkyn et al., 2002; Yucesoy et al., 2002) in which the strain energy is defined as a function of individual components of the Green-Lagrange strain. In this case, the energies for each component can more explicitly represent the tissue structure; however, the strain energy depends on the definition of a fiber axis (as in transverse isotropy) and two material axes in the plane perpendicular to the fiber axis. Therefore, transverse isotropy cannot be represented using the orthotropic formulation. Our formulation allows for explicit and independent representation of the material's resistance to along-fiber and cross-fiber shear, without the dependence on the definition of the transverse material axes.

Several aspects of muscle structure not included in our model could also influence the strain distributions in the biceps brachii. Our model incorporates only the quasi-static elastic properties of muscle tissue. Dynamic effects, such as sarcomere popping, have been shown to create nonuniform sarcomere lengths along individual

fibers (Morgan, 1990). However, these dynamic effects may not play a major role in the biceps because this muscle primarily operates in the ascending limb of the force–length curve (Murray et al., 2000), and sarcomere popping is a most prevalent in the descending limb of the force–length curve. In addition, our model uses a constant value for the maximum isometric stress and activation level, assuming that the spatial distribution of motor units and are uniform within the muscle. These effects could be sources for nonuniform shortening along muscle fibers. However, our model shows that the quasi-static mechanical properties, in the context of the complex fascicle geometry, can explain the nonuniform strains observed in the experimental data. Future work that incorporates the dynamic effects could evaluate their relative contributions to nonuniform strains in muscle.

Representation of muscle as a continuum with complex fascicle geometry introduces a new set of parameters for which little experimental data are available. While some of the material properties have been measured (e.g., force–length behavior of a fiber), data describing other properties have not been determined experimentally (e.g., the resistance to along-fiber and cross-fiber shear). Therefore, we began by using a linear shear stress–strain relationship. We selected shear modulus values that were within a physiological range and resulted in strain distributions that were consistent with the in vivo data in the biceps brachii. We found that the local strain distributions were sensitive to the shear properties. However, the relative influences of the various geometrical features (variation in fascicle length, fascicle curvature, aponeruosis stretch) were not affected by large variations (two orders of magnitude) in the shear properties, indicating that our overall conclusions are robust. We expect the shear properties to vary across muscles, as the amount and structure of the intramuscular connective tissues vary significantly across muscles. The constitutive model that we present provides a theoretical basis for future experiments that could combine imaging measurements with in vitro mechanical testing that may identify more complex shear stress–strain relationships. We also assumed a variation in fascicle lengths, consistent with measurements from ultrasound and MR (Asakawa et al., 2002). Though data do exist for the average optimal fiber length in the muscle (Murray et al., 2000), no robust data exist that characterize the variation in optimal fiber lengths within the biceps brachii. Detailed architecture measurements that capture the fiber trajectories in the muscle and the distribution of optimal fiber lengths are needed.

Combining computational modeling and dynamic image data can deepen our understanding of how individual muscle fibers interact and function within whole muscle. While we focused on the geometry of the biceps brachii, the techniques introduced here could be used to study a wide range of muscle architectures. Since fascicle arrangement and passive structures vary greatly across muscle architectures (Alexander and Ker, 1990), the theoretical framework presented in this paper could potentially enhance our understanding of the effects of muscle architecture on normal muscle function. Moreover, muscle pathologies are often manifested by alterations in fibers (Tardieu et al., 1982), connective tissue (Lieber et al., 2003), and passive structures (Shortland et al., 2002). Analyzing muscles using this theoretical framework could also help us understand how these alterations due to pathology affect muscle function.

Acknowledgements

We are thankful to Jeff Weiss, George Pappas, Deanna Asakawa, and the Lawrence Livermore National Labs. Funding for this work was provided by the National Institutes of Health Grant HD38962, a graduate fellowship from the National Science Foundation, and a Stanford Bio-X IIP grant.

Appendix

This appendix reviews the derivation of Eq. (6). We begin by defining the Cauchy stress ($\sigma_{\text{total}}^{\text{fiber}}$) generated by contraction in the fiber bundle with maximum force ($F_{\max}$) with cross sectional area (a) and activation level (α):

$$\sigma_{\text{total}}^{\text{fiber}}(\lambda) = F_{\max} f_{\text{total}}^{\text{fiber}}(\lambda, \alpha)/a(\lambda). \tag{A.1}$$

The expression (A.1) relates the maximum force and the cross-sectional area to the Cauchy stress. To generalize this equation, we assume that when fibers have stretched to optimal fiber length (λ_{ofl}), the maximum isometric stress ($\sigma_{\max}$) is

$$\sigma_{\max} = F_{\max}/a(\lambda_{\text{ofl}}). \tag{A.2}$$

The maximum isometric stress in muscle has been determined in a number of ways (e.g., Zajac, 1989 for review). Combining Eqs. (A.2) and (A.1)

$$\sigma_{\text{total}}^{\text{fiber}}(\lambda, \alpha) = \sigma_{\max} f_{\text{total}}^{\text{fiber}}(\lambda, \alpha)\, a(\lambda_{\text{ofl}})/a(\lambda). \tag{A.3}$$

The change in cross-sectional area from the undeformed configuration to the deformed configuration can be expressed in terms of J and λ (as derived from Criscione et al., 2001, Eq. 3.6)

$$a(\lambda)/a(\lambda = 1.0) = J^{1/3}/\lambda. \tag{A.4}$$

Since our model is incompressible, we will assume $J = 1$. Using (A.4), we define the area at any arbitrary λ and at

λ_{ofl}, and the ratio between these areas

$$a(\lambda) = a(\lambda = 1.0)/\lambda, a(\lambda_{ofl}) = a(\lambda = 1.0)/\lambda_{ofl},$$
$$a(\lambda_{ofl})/a(\lambda) = \lambda/\lambda_{ofl}. \quad (A.5)$$

Substituting (A.5) into (A.3), we arrive at an Eq. (6):

$$\sigma^{fiber}_{total}(\lambda, \alpha) = \sigma_{max} f^{fiber}_{total}(\lambda, \alpha)\lambda/\lambda_{ofl}. \quad (A.6)$$

References

Ahn, A.N., Monti, R.J., Biewener, A.A., 2003. In vivo and in vitro heterogeneity of segment length changes in the semimembranosus muscle of the toad. Journal of Physiology 549, 877–888.

Alexander, R.M., Ker, R.F., 1990. The architecture of leg muscles. In: Winters, J. M., Woo, S. L. (Eds.), Multiple Muscle Systems. Springer, New York, pp. 568–577.

Asakawa, D.S., Pappas, G.P., Delp, S.L., Drace, J.E., 2002. Aponeurosis length and fascicle insertion angles of the biceps brachii. Journal of Mechanics and Medicine in Biology Vol. 2, 449–455.

Criscione, J.C., Douglas, A.S., Hunger, W.C., 2001. Physically based strain invariant set for materials exhibiting transversely isotropic behavior. Journal of the Mechanics and Physics of Solids 49, 871–897.

Denoth, J., Stussi, E., Csucs, G., Danuser, G., 2002. Single muscle fiber contraction is dictated by inter-sarcomere dynamics. Journal of Theoretical Biolology 216, 101–122.

Drost, M.R., Maenhout, M., Willems, P.J., Oomens, C.W., Baaijens, F.P., Hesselink, M.K., 2003. Spatial and temporal heterogeneity of superficial muscle strain during in situ fixed-end contractions. Journal of Biomechanics 36, 1055–1063.

Gardiner, J.C., Weiss, J.A., 2001. Simple shear testing of parallel-fibered planar soft tissues. Journal of Biomechanical Engineering 123, 170–175.

Gielen, A.W., Oomens, C.W., Bovendeerd, P.H., Arts, T., Janssen, J.D., 2000. A finite element approach for skeletal muscle using a distributed moment model of contraction. Computer Methods in Biomechanics and Biomedical Engineering 3, 231–244.

Gordon, A.M., Huxley, A.F., Julian, F.J., 1966. The variation in isometric tension with sarcomere length in vertebrate muscle fibres. Journal of Physiology 184, 170–192.

Huijing, P.A., 1999. Muscle as a collagen fiber reinforced composite: a review of force transmission in muscle and whole limb. Journal of Biomechanics 32, 329–345.

Jenkyn, T.R., Koopman, B., Huijing, P., Lieber, R.L., Kaufman, K.R., 2002. Finite element model of intramuscular pressure during isometric contraction of skeletal muscle. Physics Medicine and Biology 47, 4043–4061.

Johansson, T., Meier, P., Blickhan, R., 2000. A finite-element model for the mechanical analysis of skeletal muscles. Journal of Theoretical Biology 206, 131–149.

Lieber, R.L., Runesson, E., Einarsson, F., Friden, J., 2003. Inferior mechanical properties of spastic muscle bundles due to hypertrophic but compromised extracellular matrix material. Muscle Nerve 28, 464–471.

Martins, J.A.C., Pires, E.B., Salvado, R., Dinis, P.B., 1998. A numerical model of passive and active behavior of skeletal muscles. Computer Methods in Applied Mechanics and Engineering 151, 419–433.

Morgan, D.L., 1990. New insights into the behavior of muscle during active lengthening. Biophysics Journal 57, 209–221.

Murray, W.M., Buchanan, T.S., Delp, S.L., 2000. The isometric functional capacity of muscles that cross the elbow. Journal of Biomechanics 33, 943–952.

Oomens, C.W., Maenhout, M., van Oijen, C.H., Drost, M.R., Baaijens, F.P., 2003. Finite element modelling of contracting skeletal muscle. Philosophical Transactions of the Royal Society of London, series B: Biological Sciences 358, 1453–1460.

Pappas, G.P., Asakawa, D.S., Delp, S.L., Zajac, F.E., Drace, J.E., 2002. Nonuniform shortening in the biceps brachii during elbow flexion. Journal of Applied Physiology 92, 2381–2389.

Purslow, P.P., 2002. The structure and functional significance of variations in the connective tissue within muscle. Comparative Biochemistry and Physiology, Part A, Molecular and Integrative Physiology 133, 947–966.

Puso, M.A., Maker, B.N., Ferencz, R.M., Hallquist, J.O., 2002. Nike3d: a nonlinear, implicit, three-dimensional finite element code for solid and structural mechanics. Lawrence Livermore National Lab Technical Report, UCRL-MA-105268.

Sandercock, T.G., 2003. Nonlinear summation of force in cat tibialis anterior: a muscle with intrafascicularly terminating fibers. Journal of Applied Physiology 94, 1955–1963.

Shortland, A.P., Harris, C.A., Gough, M., Robinson, R.O., 2002. Architecture of the medial gastrocnemius in children with spastic diplegia. Developmental Medicine and Child Neurology 44, 158–163.

Simo, J.C., Taylor, R.L., 1991. Quasi-incompressible finite elasticity in principal stretches: continuum basis and numerical examples. Computer Methods in Applied Mechanics and Engineering 51, 273–310.

Street, S.F., 1983. Lateral transmission of tension in frog myofibers: a myofibrillar network and transverse cytoskeletal connections are possible transmitters. Journal of Cell Physiology 114, 346–364.

Tardieu, C., Huet de la Tour, E., Bret, M.D., Tardieu, G., 1982. Muscle hypoextensibility in children with cerebral pal. Clinical and experimental observations. Archievs of Physical Medicine and Rehabilitation 63, 97–102.

Trotter, J.A., 1990. Interfiber tension transmission in series-fibered muscles of the cat hindlimb. Journal of Morphology 206, 351–361.

Trotter, J.A., 1993. Functional morphology of force transmission in skeletal muscle. A brief review. Acta Anat (Basel) 146, 205–222.

Weiss, J.A., Maker, B.N., Govindjee, S., 1996. Finite element implementation of incompressible, transversely isotropic hyperelasticity. Computer Methods in Applied Mechanics and Engineering 135, 107–128.

Yucesoy, C.A., Koopman, B.H., Huijing, P.A., Grootenboer, H.J., 2002. Three-dimensional finite element modeling of skeletal muscle using a two-domain approach: linked fiber-matrix mesh model. Journal of Biomechanics 35, 1253–1262.

Zajac, F.E., 1989. Muscle and tendon: properties, models, scaling, and application to biomechanics and motor control. Critical Reviews in Biomedical Engineering 17, 359–411.